A Review of Mutual Coupling in MIMO Systems

Chen, Xiaoming; Zhang, Shuai; Li, Qinlong

Published in:
IEEE Access

DOI (link to publication from Publisher):
10.1109/ACCESS.2018.2830653

Publication date:
2018

Document Version
Publisher's PDF, also known as Version of record

Date of publication xxxx 00, 0000, date of current version xxxx 00, 0000.

Digital Object Identifier 10.1109/ACCESS.2017.Doi Number

A Review of Mutual Coupling in MIMO Systems

Xiaoming Chen[1], Member, IEEE, Shuai Zhang[2], and Qinlong Li[3]

[1]School of Electronic and Information Engineering, Xi'an Jiaotong University, Xi'an 710049, China

[2]Antennas, Propagation and Radio Networking section at the Department of Electronic Systems, Aalborg University, Alborg 9220, Denmark

[3]Department of Electrical and Electronic Engineering, University of Hong Kong, Pokfulam Road, Hong Kong 999077, China

Corresponding author: Shuai Zhang (e-mail: sz@es.aau.dk).

This work was supported in part by InnovationsFonden project of RANGE, and also partially supported by AAU Young Talent program.

ABSTRACT This paper provides a systematic review of the mutual coupling in multiple-input multiple-output (MIMO) systems, including effects on performances of MIMO systems and various decoupling techniques. The mutual coupling changes the antenna characteristics in an array and, therefore, degrades the system performance of the MIMO system and causes spectral regrowth. Although the system performance can be partially improved by calibrating out the mutual coupling in the digital domain, it is more effective to use decoupling techniques (from the antenna point) to overcome the mutual coupling effects. Some popular decoupling techniques for MIMO systems (especially for massive MIMO base station antennas) are also presented.

INDEX TERMS Capacity, error rate, MIMO antennas, mutual coupling.

I. INTRODUCTION

Multiple-input multiple output (MIMO) techniques [1] are used ubiquitously in modern telecommunication systems, such as long-term evolution (LTE) and wireless local area network (WLAN). The massive MIMO system is believed to be a key enabler for the fifth-generation (5G) communications [2]-[4]. Due to the limited space and aesthetic reasons, compact MIMO antennas are required in mobile terminals as well as base stations (BS). As antenna elements are close to each other, (electromagnetic) mutual coupling between antenna elements becomes inevitable.

Mutual coupling in MIMO antennas arises due to free-space radiations, surface currents, and surface waves. The former two are general for all types of arrays, whereas the last one is more common for microstrip antennas. The mutual coupling can seriously degrade the signal-to-interference-noise ratio (SINR) of an adaptive array and the convergence of array signal processing algorithms [5], [6]. It can degrade the estimations of carrier frequency offset [7], channel estimation [8], and angle of arrival [9]. The adverse effect of mutual coupling on the active reflection coefficient [10] of a MIMO antenna cannot be underestimated. Due to the random phase excitations at antenna ports in MIMO transmission, the active voltage standing wave ratio (VSWR) can be as high as 6 (i.e., active reflection coefficient up to -2.92 dB) for 15-dB antenna isolation. Nevertheless, the worst active VSWR reduces to 2 if we increase the antenna isolation to 20 dB [11]. Multiple power amplifiers (PAs) in the presence of mutual coupling can cause significant out-of-band (OOB) emission [12], creating interferences to communication systems at adjacent channels. The effects of mutual coupling on error rate [13] and capacity [14] of MIMO systems are slightly more complicated. We defer the corresponding discussions to Section III.

Some efforts on mutual coupling mitigation have been exerted in the digital domain to optimize MIMO precoding and decoding schemes [14]-[16]. The mutual coupling can be removed from the received voltages [14], and then the calibrated voltages were used to compute the weight vector of adaptive algorithms [17], [18]. However, the output signal-to-interference-noise ratio (SINR) of an adaptive array cannot be improved by compensating the mutual coupling alone in post-processing [5]. (Note that the SINR can be improved by reducing the relative noise or interference in post-processing, e.g., averaging the additive noise. Nevertheless, compensating the mutual coupling does not change the SINR.) The aforementioned techniques for mitigation of mutual coupling in digital domain have a disadvantage that system performance can be only partially improved. Using decoupling techniques from the antenna point of view to overcome the mutual coupling effects are more effective. The overall mutual coupling effects on the performance of MIMO systems can be mitigated by

decoupling techniques. Therefore, it is vital to develop decoupling techniques from the antenna point of view.

The overall antenna effect (including the mutual coupling) can be mitigated by stochastic optimizations. For instances, the diversity gain of a multi-port antenna was improved using the partial swam optimization algorithms [19]; the MIMO capacity was improved by optimizing the MIMO antenna using the genetic algorithm [20], hybrid Taguchi-genetic algorithm [21], or the galaxy-based search algorithm [22]. Compared with these stochastic approaches, there is even richer literature on deterministic techniques for mutual coupling reductions. For examples, decoupling networks [23]-[26], neutralization lines [27]-[32], ground plane modifications [33]-[38], frequency-selective surface (FSS) or metasurface walls [39]-[42], metasurface corrugations or electromagnetic bandgap (EBG) structures [43], [44], and characteristic modes [45]-[48]. It should be noted that, even though the mutual coupling tends to degrade the performance of MIMO systems, it can be utilized for array calibrations [52], [53].

Review papers on mutual coupling exist in the literature [54], [55]. [54] focuses literature survey on the relationship between impedance matrix, radiation patterns, and beam coupling factors (i.e., correlations) in the presence of mutual coupling, whereas [55] provides a comprehensive review of approaches that model and mitigate the mutual coupling effect in post-processing. This paper will give a systematic review of the mutual coupling effects on MIMO systems, and popular mutual coupling reduction techniques. The mutual coupling alters antenna characteristics in an array, and thus affects the MIMO system performance (e.g., capacity, error rate, and spectral regrowth). The system performance can be partially improved by calibrating out the mutual coupling in the digital domain, but the SINR cannot be improved in post-processing by calibrating out the mutual coupling. Thus, it is important to mitigate the mutual coupling in the design of MIMO antennas, because decoupling from the antenna point can improve the overall performances for MIMO systems and makes the whole system more simple compared with techniques in digital domain. Some popular decoupling techniques for MIMO system (especially for massive MIMO BS antenna) are presented.

II. MUTUAL COUPLING

Mutual Coupling describes the energy absorbed by a nearby antenna when one antenna is operating. The mutual coupling tends to alter the input impedance, reflection coefficients, and radiation patterns of the array elements. To facilitate theoretical work, some empirical model of the mutual coupling was presented in [11],

$$C_{mn} = \exp\left(-\frac{2d_{mn}}{\lambda}(\alpha + j\pi)\right), \quad m \neq n$$
$$C_{mm} = 1 - \frac{1}{N}\sum_{m}\sum_{n\neq m} C_{mn} \tag{1}$$

where C_{mn} and d_{mn} are the mutual coupling and distance between the mth and nth antenna elements, respectively, N is the number of array elements, and α is parameter controlling the coupling level.

In practice, the mutual coupling depends not only on the array configuration but also on the excitations of other elements. It is usually quantified using the dB-valued S-parameter between the mth and nth elements, $20\log10(|S_{mn}|)$, or equivalently the isolation $-20\log10(|S_{mn}|)$ between them. Detailed mechanisms of mutual coupling depend on the transmitting/receiving mode. We discuss the mutual coupling mechanisms in the transmitting and receiving modes separately, following from [56].

A. MUTUAL COUPLING IN THE TRANSMITTING MODE

For simplifications, we consider two antenna elements m and n in an array as shown in Fig. 1. Assume a source is attached to element n, the generated energy of the source ① radiates into space ② and toward the mth element ③. Part of the energy received by the mth antenna rescatters into space ④ and the remaining travels toward the generator ⑤. A fraction of the rescattered energy ④ will be picked up by the nth element ⑥. This mutual interaction process will continue indefinitely. Nevertheless, it usually suffices to consider the first few iterations since the rescattered energy of each iteration reduces drastically. The total far-field is a vector sum of the radiated and rescattered fields. Thus, the mutual coupling tends to alter the antenna pattern. The wave ⑤ adds vectorially to the incident and reflected waves of the mth element itself, enhancing the standing wave of and, therefore, altering the input impedance of the mth element. Mutual coupling changes not only the mutual impedance but also the antenna self-impedance.

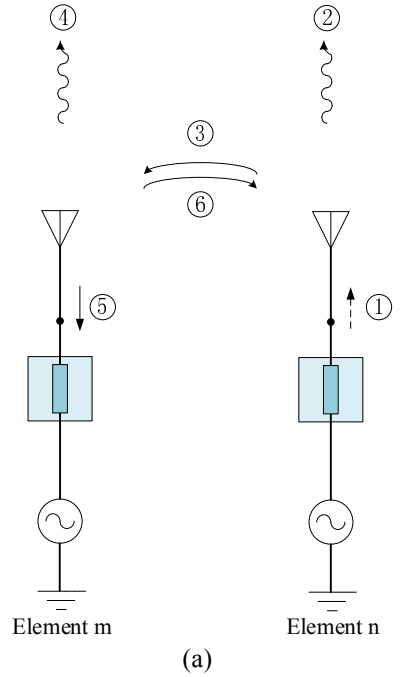

(a)

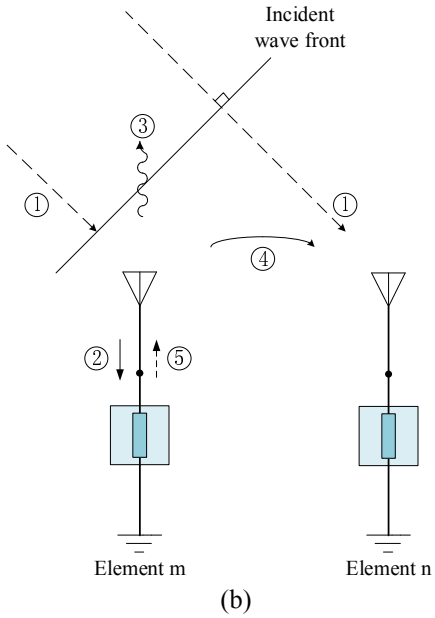

FIGURE 1. **Illustration of mutual coupling mechanisms in (a) transmitting mode and (b) receiving mode [56].**

In the transmitting mode, different ports of a multiple antenna system may have random phase excitations. It will impact both the mutual coupling and the impedance matching of antenna elements. Total active reflection coefficient (TARC) is commonly used to evaluate the reflection coefficient of a MIMO array with the random phase excitations at different element ports [83]. TARC is defined as the square root of the total generated power by all excitations minus the total radiated power, divided by the total generated power [83]. TARC takes into account impedance matching, mutual coupling and radiation efficiency under the random phase excitations at ports. Higher mutual coupling leads to worse TARC.

B. MUTUAL COUPLING IN THE RECEIVING MODE

Assume that a plane wave ① impinges onto the array, arriving at the *m*th element first. It induces a current in the *m*th element first. Part of the incident wave goes into the receiver as ②, whereas part is rescattered into space ③. Some of the rescattered wave is directed toward the *n*th element ④, where it adds vectorially with the incident plane wave ⑤. Hence, the wave received by an element is the vector sum of the direct waves and the coupled waves from other elements. In order to maximize the received energy, i.e., minimize the rescattered energy, the terminating impedance of the *m*th element should be chosen so that the resecattered wave ③ is canceled by the reflected wave ⑤.

In the receiving mode, the performance of the antenna element under investigation can be studied by exciting the element with the other element terminated with 50-ohm loads.

In the next section, we show the mutual coupling effects on MIMO systems.

III. MIMO SYSTEM IN THE PRESENCE OF MUTUAL COUPLING

Popular performance metrics for characterizing MIMO antennas are diversity gain, e.g., [51], [59], [63], [64], capacity, e.g., [14], [16], [50]-[66], throughput, e.g., [24], [67], [68], and error rate, e.g., [13], [69], [70]. Before studying the mutual coupling effects on MIMO systems, we first present a network model of the MIMO system including mutual coupling effects.

A. NETWORK MODEL

A network model of the MIMO system is given as [49]

$$\begin{bmatrix} \mathbf{v}_T \\ \mathbf{v}_R \end{bmatrix} = \begin{bmatrix} \mathbf{Z}_T & \mathbf{0} \\ \mathbf{H}^{oc} & \mathbf{Z}_R \end{bmatrix} \begin{bmatrix} \mathbf{i}_T \\ \mathbf{i}_R \end{bmatrix} \tag{2}$$

where $\mathbf{Z}_T$ ($\mathbf{Z}_R$), $\mathbf{i}_T$ ($\mathbf{i}_R$), and $\mathbf{v}_T$ ($\mathbf{v}_R$) are impedance matrix, current and voltage vectors at the transmitter (receiver), respectively; $\mathbf{0}$ is zero matrix with proper dimensions, $\mathbf{H}^{oc}$ is the open-circuit MIMO channel matrix. It is noted that, for notation simplicity and without loss of generality, the additive noises is omitted for the time being, while it can be easily included afterwards.

Based on simple circuit theory, the transmit and receive voltage vectors can be written as

$$\begin{aligned} \mathbf{v}_T &= \mathbf{Z}_T(\mathbf{Z}_T + \mathbf{Z}_s)^{-1}\mathbf{v}_s \\ \mathbf{v}_R &= -\mathbf{Z}_L\mathbf{i}_R \end{aligned}, \tag{3}$$

respectively, where $\mathbf{v}_s$ is source voltage vector, $\mathbf{Z}_s$ and $\mathbf{Z}_L$ are source and load impedance matrices, respectively. $\mathbf{v}_R$ can be expressed in terms of $\mathbf{v}_T$ as

$$\mathbf{v}_R = \mathbf{Z}_L(\mathbf{Z}_L + \mathbf{Z}_R)^{-1}\mathbf{H}^{oc}(\mathbf{Z}_T + \mathbf{Z}_s)^{-1}\mathbf{v}_s. \tag{4}$$

The term $\mathbf{Z}_L(\mathbf{Z}_L + \mathbf{Z}_R)^{-1}\mathbf{H}^{oc}(\mathbf{Z}_T + \mathbf{Z}_s)^{-1}$ is a voltage transfer function. In order to relate it to the information-theoretic input-output relation $\mathbf{y} = \mathbf{H}\mathbf{x}$, (4) has to be properly normalized so that the received power satisfies $E\{tr[\mathrm{Re}(\mathbf{Z}_L\mathbf{i}_R\mathbf{i}_R^H)]\} = E[tr(\mathbf{y}\mathbf{y}^H)] = E[tr(\mathbf{H}_{eff}\mathbf{K}_x\mathbf{H}_{eff}^H)]$, where $\mathbf{K}_x = \mathbf{I}_{N_t}P_T / N_t$ is covariance matrix of the transmit signals and $P_T = E\{tr[\mathrm{Re}(\mathbf{Z}_T\mathbf{i}_T\mathbf{i}_T^H)]\}$. Let $\mathbf{R}_L$=Re$\{\mathbf{Z}_L\}$ and $\mathbf{R}_T$=Re$\{\mathbf{Z}_T\}$, the effective channel can be derived as

$$\mathbf{H}_{eff} = \sqrt{N_t}\mathbf{R}_L^{1/2}(\mathbf{Z}_L + \mathbf{Z}_R)^{-1}\mathbf{H}^{oc}\mathbf{R}_T^{-1/2}. \tag{5}$$

The effective channel should be normalized to the average channel gain of a single-antenna system with antennas at both side conjugate matched, i.e. $z_L = z_R^*$ and $z_s = z_T^*$, where z_T and z_R are antenna impedance at the transmit and receive sides, respectively, and z_L and z_s are load and source impedances at transmit and receive sides, respectively. It is easy to show that the effective SISO channel is

$$h_{eff} = \sqrt{\frac{N_t}{r_R r_T}} \frac{h}{2} \tag{6}$$

where $r_T = \mathrm{Re}\{z_T\}$, $r_R = \mathrm{Re}\{z_R\}$ and $E[|h|^2] = 1$. Dividing $\mathbf{H}_{eff}$ with $\sqrt{E[|h_{eff}|^2]}$, the normalized MIMO channel that includes overall antenna effect is [50]

$$\mathbf{H} = 2\sqrt{r_R r_T}\,\mathbf{R}_L^{1/2}(\mathbf{Z}_L + \mathbf{Z}_R)^{-1}\mathbf{H}^{oc}\mathbf{R}_T^{-1/2} \tag{7}$$

where $\mathbf{H}^{oc} = \mathbf{\Phi}_R^{oc,1/2}\mathbf{H}_w\mathbf{\Phi}_T^{oc,1/2}$, with $\mathbf{\Phi}_R^{oc}$ and $\mathbf{\Phi}_R^{oc}$ denoting the open-circuit correlation matrix.

B. MUTUAL COUPLING ON ANTENNA CHARACTERISTICS

For simplicity, we resort to the example of parallel half-wavelength dipoles (see Fig. 2).

The mutual impedance is defined as the ratio of the open-circuit voltage at one port to the induced current at the other port,

$$Z_{12} = \left.\frac{V_1}{I_2}\right|_{I_1=0}. \tag{8}$$

The mutual impedance as a function of dipole separation (normalized by the wavelength) is shown in Fig. 3. As can be seen, the mutual impedance is non-negligible at small dipole separation yet tends to approach zero as the dipole separation increases.

The self-impedance Z_{11} is defined as the ratio of the voltage to the current when the other port is open-circuited,

$$Z_{11} = \left.\frac{V_1}{I_1}\right|_{I_2=0}. \tag{9}$$

An open-circuited single mode small antenna (e.g., dipole) is electromagnetically invisible [58]. Therefore, Z_{11} can be well approximated by the input impedance of a half-wavelength dipole, i.e., Z_{11} = 73+j42.5 ohms. Since the two dipoles are identical, $Z_{11} = Z_{22}$. Due to the reciprocity, $Z_{12} = Z_{21}$.

Assume the two dipoles are located at y_1=-d/2 and y_2=d/2 along the y-axis, respectively (cf. Fig. 2). When one dipole is open-circuited, the far-field function of the other half-wavelength dipole can be well approximated by the isolated far-field function as

$$\mathbf{g}_i(\theta,\phi) = \left[-\frac{2C_k\eta\cos(\pi/2\cos\theta)}{k\sin\theta}\exp(jk\frac{d_i}{2}\sin\theta\sin\phi) \quad 0\right]^T$$

$$= \left[g_i(\theta,\phi) \quad 0\right]^T \tag{10}$$

where i =1, 2, d_1=-d, d_2=d, $k = 2\pi/\lambda$, $C_k = -jk/4\pi$, the superscript ^{T} denotes transpose, and η is free space wave impedance. When one dipole is terminated with a load Z_L, the far-field function of the other dipole is [59]

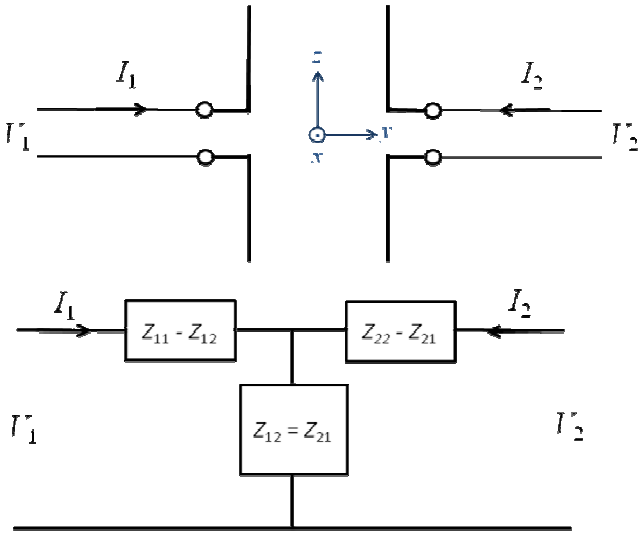

FIGURE 2. Illustration of parallel dipoles and their equivalent circuit.

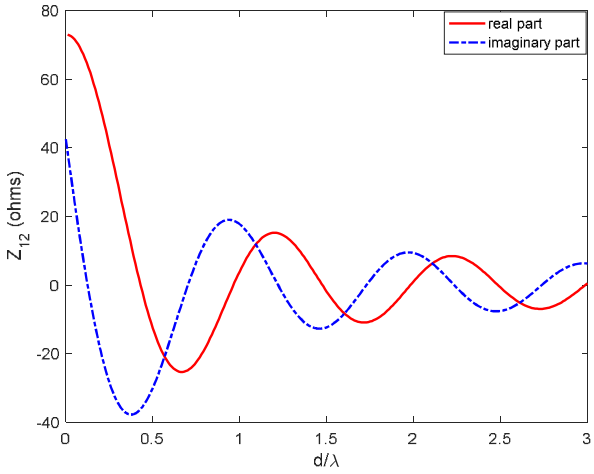

FIGURE 3. The mutual impedance of parallel half-wavelength dipoles as a function of dipole separation [57].

$$\mathbf{g}_{emb,i}(\theta,\phi) = \mathbf{g}_i(\theta,\phi)I_i + \mathbf{g}_{(i+1)_{\mathrm{mod}\,2}}(\theta,\phi)I_{(i+1)_{\mathrm{mod}\,2}}, \tag{11}$$

where mod2 is the modulo operator with 2 as the divisor. From the equivalent circuit (cf. Fig. 2), when the excitation current at port 1 is unity, i.e., I_1=1, the induced current at port 2 is I_2=-Z_{12}/(Z_{22}+ Z_L). Equation (11) is referred to as embedded far field function [59].

To show the mutual coupling effect on antenna patterns, we plot the antenna pattern of an isolated dipole, the embedded antenna patterns of parallel dipoles with quarter-wavelength separation in Fig. 4. As can be seen, the antenna pattern of an isolated dipole is omni-directional and the parallel dipoles tend to radiate outwards by virtual of the mutual coupling. It is evident that the mutual coupling alters the antenna pattern.

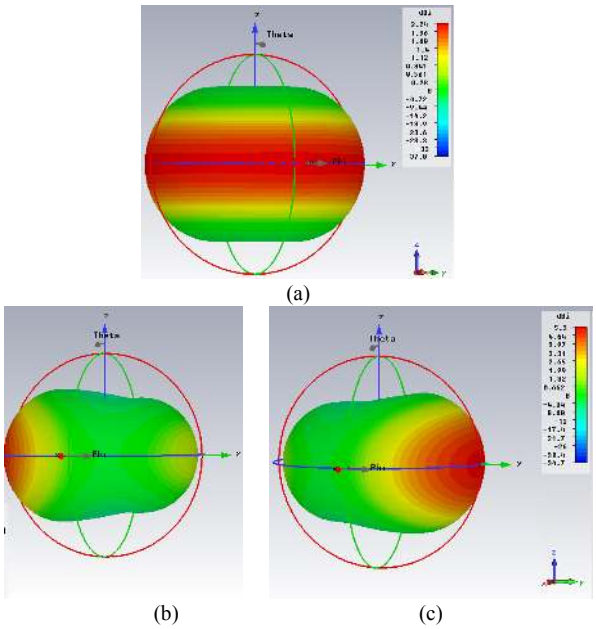

(a) (b) (c)

FIGURE 4. Antenna patterns: (a) isolated antenna pattern; (b) embedded antenna pattern of the left dipole; (c) embedded antenna pattern of the right dipole. Dipole separation is quarter-wavelength.

The correlation between the dipoles can be calculated as [62]

$$\frac{\iint_{4\pi} \mathbf{g}_{emb,1}^{H}(\Omega)\mathbf{P}_a(\Omega)\mathbf{g}_{emb,2}(\Omega)d\Omega}{\sqrt{\iint_{4\pi} \mathbf{g}_{emb,1}^{H}(\Omega)\mathbf{P}_a(\Omega)\mathbf{g}_{emb,1}(\Omega)d\Omega \cdot \iint_{4\pi} \mathbf{g}_{emb,2}^{H}(\Omega)\mathbf{P}_a(\Omega)\mathbf{g}_{emb,2}(\Omega)d\Omega}} \tag{12}$$

where the superscript ^{H} denotes Hermitian, Ω is the solid angle of arrival, and $\mathbf{P}_a$ is the dyadic power angular spectrum of the incident waves. When the angular spectrum is unknown a priori, the isotropic scattering condition, i.e., $\mathbf{P}_a(\Omega) = \mathbf{I}$, is usually assumed.

Another way to calculate the correlation is to use the self and mutual impedances explicitly. The received voltages in the presence of mutual coupling can be expressed as

$$\mathbf{v} = \mathbf{Z}_{\mathrm{L}}[\mathbf{Z} + \mathbf{Z}_{\mathrm{L}}]^{-1}\mathbf{v}_{oc} \tag{13}$$

where $\mathbf{v}_{oc} = [v_1^{oc} \quad v_2^{oc}]^T$ and $\mathbf{v} = [v_1 \quad v_2]^T$ are open-circuit voltages and voltages with mutual coupling, respectively, $\mathbf{Z}_{\mathrm{L}}$ is a diagonal matrix whose diagonal entries are the identical load impedance Z_{L}, and $\mathbf{Z}$ is the impedance matrix for the parallel dipoles. Equation (13) can be rewritten as

$$\begin{bmatrix} v_1 \\ v_2 \end{bmatrix} = \begin{bmatrix} \alpha & \beta \\ \beta & \alpha \end{bmatrix} \begin{bmatrix} g_1(\theta,\phi) \\ g_2(\theta,\phi) \end{bmatrix} \tag{14}$$

where α and β are the corresponding entries of the coupling matrix $\mathbf{Z}_{\mathrm{L}}[\mathbf{Z} + \mathbf{Z}_{\mathrm{L}}]^{-1}$ and the far-field function $g_2(\theta,\phi) = g_1(\theta,\phi)\exp(jkd\cos\phi)$. The correlation with mutual coupling is

$$\rho = \frac{E[v_1 v_2^*]}{\sqrt{E[|v_1|^2]E[|v_2|^2]}}$$

$$= \frac{(|\alpha|^2 + |\beta|^2)\Im\{\rho_{oc}\} + 2\Re\{\alpha\beta^*\} + j(|\alpha|^2 - |\beta|^2)\Im\{\rho_{oc}\}}{\sqrt{E[|v_1|^2]E[|v_2|^2]}} \tag{15}$$

where the superscript * represents complex conjugate and E denotes expectation. The terms in the denominator of (15) can be expressed as

$$E[|v_1|^2] = |\alpha|^2 + |\beta|^2 + 2\Re\{\rho_{oc}\}\Re\{\alpha\beta^*\} + 2\Im\{\rho_{oc}\}\Im\{\alpha\beta^*\}$$
$$E[|v_2|^2] = |\alpha|^2 + |\beta|^2 + 2\Re\{\rho_{oc}\}\Re\{\alpha\beta^*\} - 2\Im\{\rho_{oc}\}\Im\{\alpha\beta^*\} \tag{16}$$

where $\Re$ and $\Im$ denote the real and imaginary parts of their arguments, respectively, and the open-circuit correlation ρ_{oc} (i.e., the correlation without mutual coupling) can be calculated by replacing the embedded patterns with the corresponding isolated patterns.

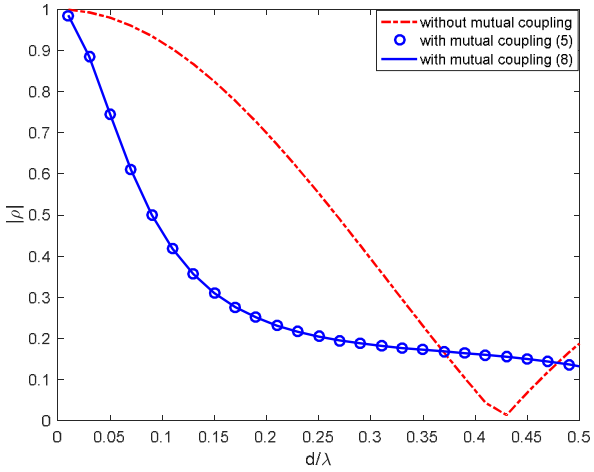

FIGURE 5. Correlations as a function of dipole separation.

Figure 5 shows the correlation has a function of dipole separation. The case without mutual coupling (open-circuit correlation) is plotted in the same figure as a reference. As can be seen, the correlation with the mutual coupling is smaller than that without mutual coupling. This is because the mutual coupling tends to make the two dipoles radiate in opposite directions (cf. Fig. 4). It can also be seen that the correlations calculated using (12) and (15) are identical. It should be noted, however, that "without mutual coupling" is just a theoretical reference case and the mutual coupling exists ubiquitously in compact MIMO antennas in practice. Comparing Figs. 3 and 5, it can be found that the mutual coupling (mutual impedance) tends to increase as the dipoles become closer (cf. Fig. 3) and that the correlation also tends to increase as the dipoles become closer (cf. Fig. 5). Hence, one may conclude that the mutual coupling tends to increase the correlation. However, when

"without mutual coupling" is used as the reference, it can be seen from Fig. 5 that the mutual coupling tends to reduce the correlation (at certain separations). The seemingly contradicting conclusions are due to the fact that different references are used. They are just two interpretations of the same phenomenon.

Since no ohmic loss is assumed in the dipoles, the energy degradation due to the mutual coupling can be characterized by the total embedded radiation efficiency

$$e_{emb} = 1 - |S_{11}|^2 - |S_{21}|^2 \tag{17}$$

where the S-parameters can be readily converted from the impedance parameters. Equation (11) takes into account of the mismatch and coupling caused by the mutual coupling. Figure 6 shows total embedded radiation efficiency (with and without mutual coupling) as a function of dipole separation. When the mutual coupling is not considered, (17) boils down to the mismatch efficiency $1-|S_{11}|^2$ (which is independent of the dipole separation). As can be seen, as the dipoles become closer, the total embedded radiation efficiency degrades.

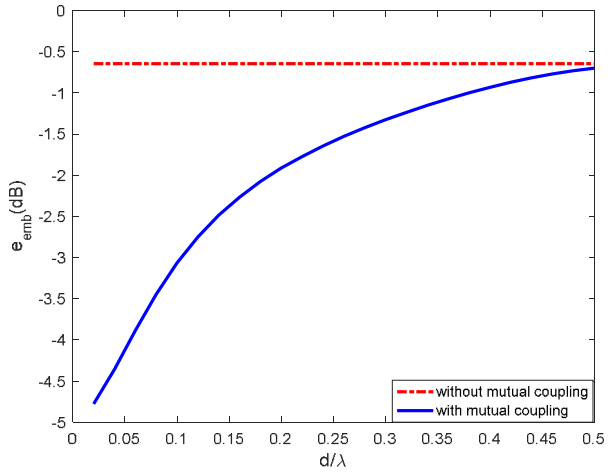

FIGURE 6. Total embedded radiation efficiency as a function of dipole separation.

It can be seen from Fig. 6 that the mutual coupling tends to reduce the total embedded radiation efficiency and, therefore, the channel gain, which degrades the performance of the MIMO system. On the other hand, Figs. 4 and 5 show that, by making the antenna pattern more orthogonal, the mutual coupling tends to reduce the antenna correlation as compared with the theoretical case when the mutual coupling is not considered. A reduction of the correlation implies an increase of the degree of freedom and a decrease of the condition number [61], which helps improve the performance of the MIMO system. As a result, the mutual coupling effect on MIMO system is not that straightforward. We resort to simulations to investigate the overall impact of mutual coupling on MIMO systems in the sequel.

C. DIVERSITY GAIN IN THE PRESENCE OF MUTUAL COUPLING

For simplicity, we first assume isotropic scattering environments and the parallel dipoles as diversity antenna [59].

The effective diversity gain is defined as the signal-to-noise ratio (SNR) improvement of a diversity gain with respect to an ideal single-port antenna [59], [63],

$$G_{eff} = \left. \frac{F^{-1}(\gamma)}{F_{ideal}^{-1}(\gamma)} \right|_{1\%} \tag{18}$$

where γ is the SNR, $(\cdot)^{-1}$ denotes functional inversion, F is the cumulative distribution function (CDF) of the output SNR of the diversity antenna, $F_{ideal}(\gamma) = 1 - \exp(-\gamma)$ is the CDF of the output SNR of the ideal single-port antenna in the Rayleigh fading environment, and the subscript 1% implies that the diversity gain is obtained at 1% CDF level. Assuming maximum ratio combining (MRC), the CDF F in (18) is

$$F(\gamma) = 1 - \frac{\xi_1 \exp(-\gamma/\xi_1) - \xi_2 \exp(-\gamma/\xi_2)}{\xi_1 - \xi_2}. \tag{19}$$

where $\xi_1 = e_{emb}(1+|\rho|)$ and $\xi_2 = e_{emb}(1-|\rho|)$ [71]. The diversity gain can be improved by reducing the correlation and increasing the embedded radiation efficiency.

Figure 7 shows the MRC diversity gain of the two parallel dipoles with and without mutual coupling as a function of dipole separation. As can be seen, the diversity gain with mutual coupling is overall lower than that without mutual coupling except at certain dipole separations (0.05~0.13λ). As mentioned before, the mutual coupling tends to reduce the correlation (as compared with the open-circuit case) and reduce the embedded radiation efficiency. The efficiency degradation is more profound than the correlation improvement, except at certain small dipole separations (0.05~0.13λ).

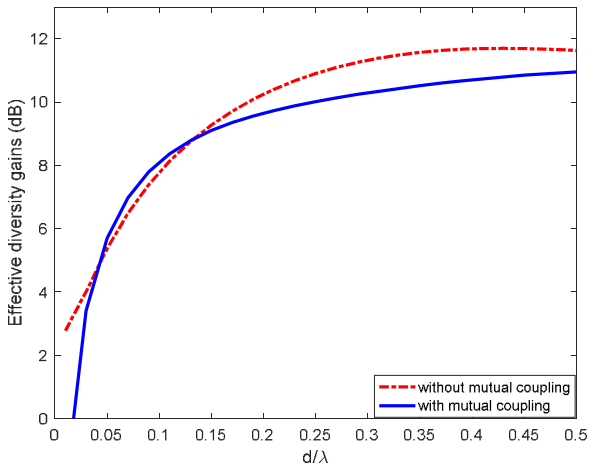

FIGURE 7. Effective diversity gain as a function of dipole separation.

D. CHANNEL CAPACITY IN THE PRESENCE OF MUTUAL COUPLING

It was claimed that the mutual coupling improves the MIMO capacity (as compared with the open-circuit case) [65]. However, the efficiency degradation due to mutual coupling was overlooked in [65]. Taking both correlation and efficiency into account, a similar conclusion can be drawn for the MIMO capacity and error rate performance [70], i.e., the mutual coupling tends to degrade the MIMO performance except at certain antenna separations.

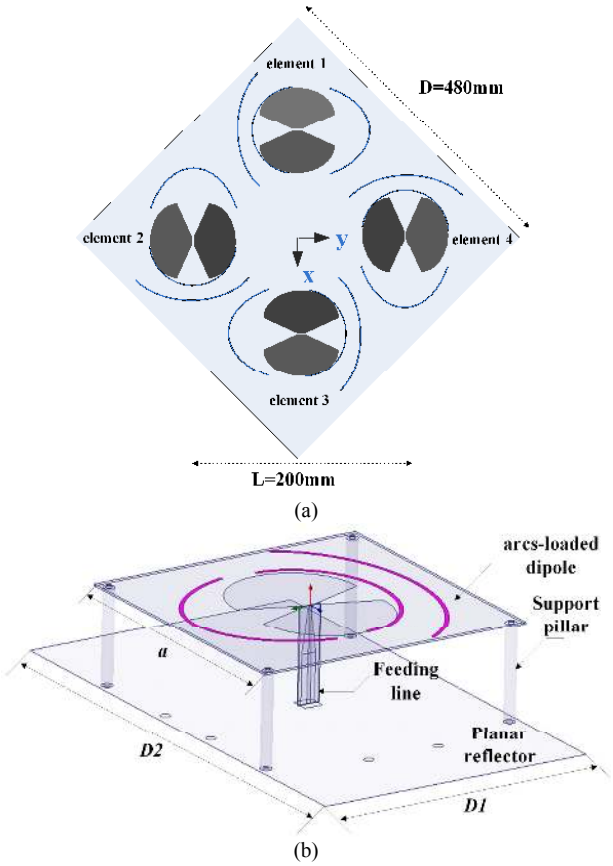

FIGURE 8. Four-port broadband MIMO antenna: (a) array configuration; (b) array element [72].

TABLE I
COUPLING COEFFICIENTS

	$\lvert S_{12}\rvert$	$\lvert S_{13}\rvert$	$\lvert S_{14}\rvert$	$\lvert S_{23}\rvert$	$\lvert S_{24}\rvert$	$\lvert S_{34}\rvert$ (dB)
0.7 GHz	-17.0	-28.6	-17.1	-17.0	-28.7	-16.9
1.7 GHz	-27.2	-26.7	-27.0	-27.1	-26.7	-27.1
2.7 GHz	-22.1	-31.6	-22.1	-22.0	-31.6	-22.0

TABLE II
CORRELATION COEFFICIENTS IN ISOTROPIC SCATTERING ENVIRONMENT [72]

	$\lvert\rho_{12}\rvert$	$\lvert\rho_{13}\rvert$	$\lvert\rho_{14}\rvert$	$\lvert\rho_{23}\rvert$	$\lvert\rho_{24}\rvert$	$\lvert\rho_{34}\rvert$
0.7 GHz	0.16	0.07	0.11	0.13	0.06	0.17
1.7 GHz	0.01	0.05	0.01	0.01	0.04	0.01
2.7 GHz	0.07	0.04	0.08	0.06	0.03	0.06

So far we have been assuming parallel dipoles. Now we consider a four-port broadband MIMO antenna (see Fig. 8) [72]. The antenna covers the frequency band of 698-2700 MHz. Its coupling coefficients are shown in Table I. As can be seen, the MIMO antenna has higher coupling in the low frequency.

In order to evaluate the performance of the broadband MIMO antenna alone, we assume two uncorrelated transmit antennas and the broadband MIMO antenna as receive antennas. We further assume that the receiver has perfect channel state information (CSI) whereas the transmitter does not. In this case, the ergodic capacity is given as [1]

$$C = E\left\{\log_2\left[\det\left(\mathbf{I}+\frac{\overline{\gamma}_0}{2}\mathbf{H}\mathbf{H}^H\right)\right]\right\} \tag{20}$$

where $\mathbf{H}$ is the (random) 4×2 MIMO channel matrix, $\mathbf{I}$ is a 4×4 identity matrix, and $\overline{\gamma}_0$ denotes the reference SNR.

For simplicity, we first assume isotropic scattering environments. The MIMO channel, in this case, can then be expressed as [50]

$$\mathbf{H} = \mathbf{R}^{1/2}\mathbf{H}_w, \tag{21}$$

where $\mathbf{H}_w$ denotes the spatially white MIMO channel with independent and identically distributed (i.i.d.) complex Gaussian entries (normalized so that its Frobenius norm satisfies $E\left[\|\mathbf{H}_w\|_F^2\right]=8$) and $\mathbf{R}^{1/2}$ is the Hermitian square root of the correlation matrix $\mathbf{R}$ of the broadband MIMO antenna. The correlation matrix is given as [73], [74]

$$\mathbf{R} = diag(\sqrt{\mathbf{e}})\mathbf{\Phi}diag(\sqrt{\mathbf{e}}) = \left(\sqrt{\mathbf{e}}\sqrt{\mathbf{e}}^T\right)\circ\mathbf{\Phi}, \tag{22}$$

where $\mathbf{\Phi}$ consists of the correlation coefficients (cf. Table II) calculated using (5), $\mathbf{e}$ denoting a column vector consisting the antenna efficiencies at the four antenna ports, $\circ$ denotes entry-wise product, and $\sqrt{\ }$ denotes the entry-wise square root. Combining (20)-(22), the ergodic capacity can be rewritten as

$$\begin{aligned} C &= E\left\{\log_2\left[\det\left(\mathbf{I}+\frac{\overline{\gamma}_0}{2}(\mathbf{R}^{1/2}\mathbf{H}_w)(\mathbf{R}^{1/2}\mathbf{H}_w)^H\right)\right]\right\} \\ &= E\left\{\log_2\left[\det\left(\mathbf{I}+\frac{\overline{\gamma}_0}{2}\mathbf{R}\mathbf{H}_w\mathbf{H}_w^H\right)\right]\right\}. \end{aligned} \tag{23}$$

Figure 9 shows the simulated MIMO capacities of the MIMO antenna at different frequencies calculated using 100000 channel realizations in an isotropic scattering environment. As a reference, the ideal case with i.i.d. MIMO channel is also plotted in the same figure. As can be seen, the capacities at different frequencies overlap with each other and that the proposed MIMO antenna incurs little impairment on the MIMO capacity in the isotropic scattering environment.

The isotropic scattering environment is a special extreme scenario. In order to evaluate the MIMO capacity in a more representative multipath environment, we resort to the WINNER+ channel model [75]. The WINNER+ model is a geometry-based stochastic channel model [76], [77], which has been validated and calibrated by extensive

measurements for different scenarios. The indoor hotspot scenario is chosen here. For simplicity, we assume the transmitter is equipped with orthogonal polarized half-wavelength dipoles so that the transmitting antennas are uncorrelated. For channel simulations, the antenna patterns are first imported into the model; for each drop (realization), 10 random clusters (paths) with different path gains, delays, and mean angles with respect to (w.r.t.) the antennas are generated; each cluster is further modeled by 20 sub-clusters with different sub-angle but indistinguishable delays. In total, 10000 channel realizations are generated.

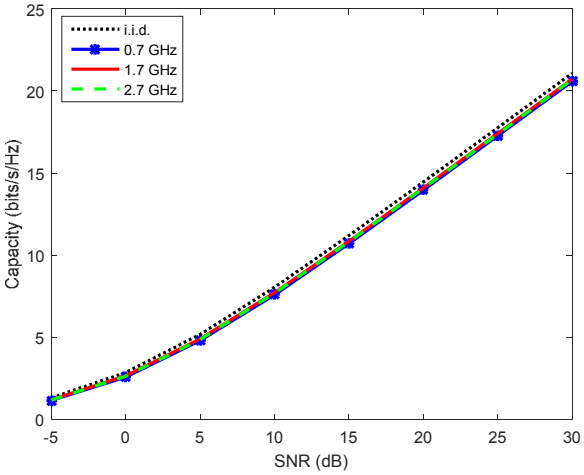

FIGURE 9. Simulated MIMO capacities of the MIMO antenna at different frequencies in isotropic scattering environment [72].

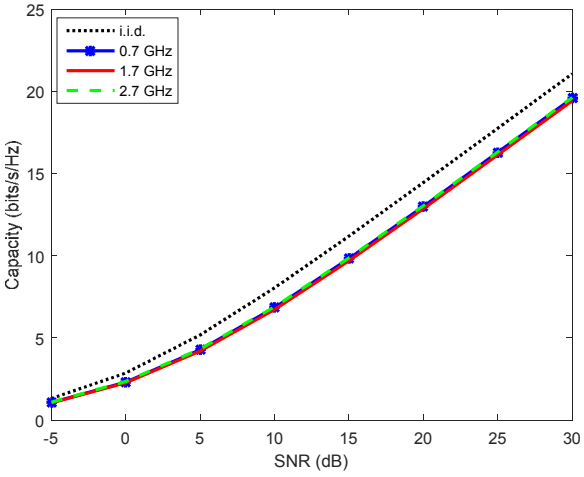

FIGURE 10. Simulated MIMO capacities of the MIMO antenna at different frequencies in WINNER indoor hotspot scenario [72].

Figure 10 shows the simulated MIMO capacities in the indoor hotspot scenario. As in the isotropic scattering environment, the MIMO capacities at 0.7, 1.7 and 2.7 GHz overlap. Nevertheless, there is noticeable capacity degradation as compared to the ideal case (with i.i.d. MIMO channel). This degradation is due to increased correlation and power imbalance in the indoor hotspot scenario [78]. The transmit antennas have negligible correlation thanks to the orthogonal dipoles. Yet the correlations at the broadband MIMO antenna increase due to the non-uniform angular distribution. (The maximum angular spread is 63°[79] at the broadband MIMO antenna.) The highest correlation magnitude becomes 0.33. It is shown that small correlation of 0.3 can still incur a noticeable degradation of the MIMO capacity when the number of antenna elements exceeds three [80]. The maximum cross polarization discrimination (XPD) in the WINNER indoor hotspot scenario is around 10 dB [79]. Since the broadband MIMO antenna is dual-polarized (cf. Fig. 8), actual power imbalance according to the simulations is below 2.5 dB (which can result in 1.5-dB capacity degradation [73]).

Given the fact that the mutual coupling at 0.7, 1.7, and 2.7 GHz is about -17, -27, and -22 dB, respectively, and that the MIMO capacities are about the same at these frequencies, it is evident that mutual coupling below -17 dB has negligible impact on the MIMO capacity. There seems no point of further improving the mutual coupling below -17 dB.

E. ERROR RATE IN THE PRESENCE OF MUTUAL COUPLING

A myth about mutual coupling on the error rate performance is that the high modulation (e.g., 256-QAM) transmission require about an SNR of about 30 dB in additive white Gaussian noise (AWGN) channel and, therefore, the mutual coupling should be below -30 dB.

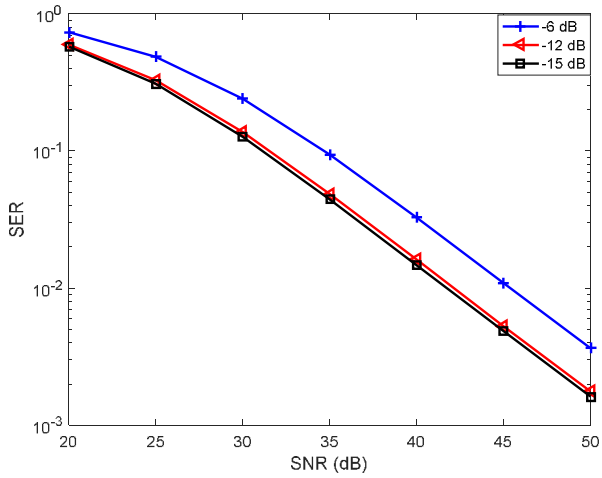

FIGURE 11. SER performance of a 2×2 MIMO-OFDM system under different mutual coupling.

In MIMO spatial multiplexing (i.e., transmission of multiple data streams simultaneously over the same bandwidth), the received signal at each antenna port is a mixture of all the transmitted signals by virtual of multipath propagation as well as mutual coupling, i.e., the mutual coupling is part of the MIMO channel. MIMO decoders are usually used to decouple composite MIMO channel (i.e., not only the propagation channels but also the mutual coupling).

To demonstrate this, we assume a 2×2 MIMO system with uncorrelated transmit antennas and parallel dipoles as receive antennas in a multi-tap Rayleigh fading channel with a channel length of 60. The orthogonal frequency division multiplexing (OFDM) with 1024 subcarriers is used to mitigate the delay spread of the propagation channel. The subcarriers are loaded with 256-QAM symbols. For simplicity and to focus on the mutual coupling effect, we set the cyclic prefix (CP) of the OFDM to be 64 (i.e., longer than the channel length) and assume the MIMO channel can be estimated perfectly. (In practice, the channel can be accurately estimated using the preamble.) Figure 11 shows the symbol error rate (SER) performance of the MIMO-OFDM system under different mutual coupling levels. (Note that, by convention, the SNR in the error rate plot is defined as the ratio of the transmit signal power to the noise power. In simulations, different SNRs were emulated by varying the noise power.) As can be seen, the 256-QAM symbol can be detected at the high mutual coupling. As we improve the mutual coupling from -6 to -12 dB (by increasing the antenna separation), the SER performance improve by 3 dB approximately. Improving the mutual coupling from -12 to -15 dB results in only marginal improvement of the SER performance and there is little SER improvement by improving mutual coupling further. Therefore, -15 dB mutual coupling is sufficient for MIMO transmission from the error rate point of view.

F. SPECTRAL REGROWTH IN THE PRESENCE OF MUTUAL COUPLING AND PA NONLINEARITY

Apart from degradation of diversity gain, capacity, error rate performance of MIMO systems, the mutual coupling together with PA nonlinearity also results in spectral regrowth, i.e., an increase of out-of-band (OOB) emission [12], [81].

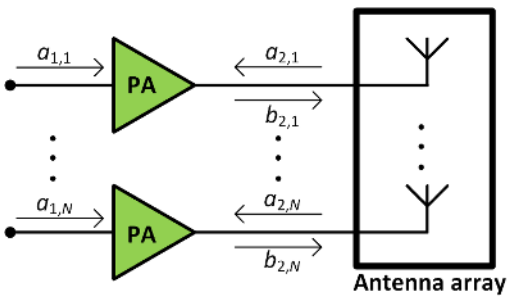

FIGURE 12. Illustration of a MIMO transmitter with PAs [12].

Figure 12 is an illustration of a MIMO transmitter with N branches and a PA per branch. The incident wave to the PA in the ith branch is denoted as $a_{1,i}$. The output wave of the PA $b_{2,i}$ feeds into the ith antenna element. The impedance mismatch between the PA and the antenna element and the mutual coupling between antenna elements result in a reflected wave $a_{2,i}$ back to the output of the PA in the ith branch. The dual-input nonlinear dynamic model of the MIMO transmitter is given as [12]

$$b_2[n]=\underbrace{\sum_{m_1=0}^{M_1}\sum_{p_1=1}^{P_1}\alpha_{m_1}^{p_1}(T_n)\left|a_1[n-m_1]\right|^{2(p_1-1)}}_{S_{21}(|a_1|,T)}a_1[n-m_1]+$$
$$\underbrace{\sum_{m_2=0}^{M_2}\sum_{m_1=0}^{M_1}\sum_{p_2=1}^{P_2}\beta_{m_1m_2}^{p_2}(T_n)\left|a_1[n-m_1]\right|^{2(p_2-1)}}_{S_{22}(|a_1|,T)}a_2[n-m_2]+$$
$$\underbrace{\sum_{m_2=0}^{M_2}\sum_{m_1=0}^{M_1}\sum_{p_2=2}^{P_2}\gamma_{m_1m_2}^{p_2}(T_n)a_1^2[n-m_1]\left|a_1[n-m_1]\right|^{2(p_2-2)}}_{T_{22}(a_1,T)}a_2^*[n-m_2] \tag{24}$$

where $\alpha_{m_1}^{p_1}$, $\beta_{m_1m_2}^{p_2}$, and $\gamma_{m_1m_2}^{p_2}$ are modeling parameters to be extracted from measurements. The total far-field function of the MIMO transmitter is

$$\mathbf{g}_{total}(\theta,\phi)=\sum_{i=1}^{N}b_{2,i}\mathbf{g}_i(\theta,\phi)\,. \tag{25}$$

An illustration of the effects of mutual coupling and PA nonlinearity on OOB emission (or spectral regrowth) is shown in Fig. 13. As the mutual coupling increases (i.e., isolation decreases), the OOB emission increases. To quantify the OOB emission, the adjacent channel power ratio (ACPR), i.e., the ratio between the total leakage power to adjacent channels to the in-band power.

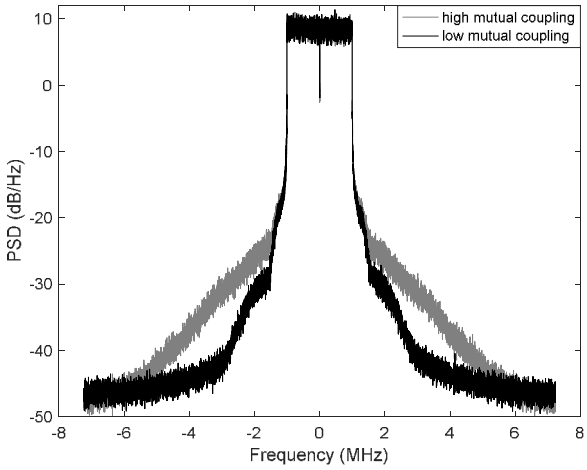

FIGURE 13. Illustration of spectral regrowth due to mutual coupling and PA nonlinearity.

TABLE III
SPECTRAL REGROWTH DUE TO MUTUAL COUPLING AND PA NONLINEARITY [12]

Antenna separation	mutual coupling	ACPR
0.36 λ	-14.0 dB	-46.4 dBc
0.44 λ	-20.9 dB	-52.3 dBc
0.59 λ	-28.4 dB	-57.4 dBc

The authors in [12] demonstrate the effects of mutual coupling and PA nonlinearity on spectral regrowth by varying the separation between two path antennas (i.e., the

mutual coupling level) and measuring the power spectral density (PSD) of the MIMO transmitter with two identical PAs (CGH40006S-TB) at 2. 14 GHz. (The PA has 65% efficiency and third order intermodulation distortion of about -40 dBc with an input power of 32 dBm.) The results are summarized in Table III. Even though there are only marginal improvements on capacity and error rate performances by improving the mutual coupling below -15 dB, further improvement of the mutual coupling below -15 dB can effectively reduce the OOB emission and, therefore, reduce the interference to the adjacent channel.

Note that, in addition to spectral regrowth, the PA nonlinearity also causes in-band distortion with and without mutual coupling. The distorted signal can be decomposed into pure signal and perturbation. The latter can be regarded as an additional source of noise [82]. Hence, the PA nonlinearity also degrades the error rate performance.

IV. MUTUAL COUPLING REDUCTION

In this section, we discuss mutual coupling reduction (decoupling) techniques for MIMO antennas, with a special focus on decoupling techniques for massive MIMO antennas for base stations.

A. VARIOUS DECOUPLING TECHNIQUES

There are many decoupling techniques to reduce the mutual coupling in the literature. For examples, decoupling networks [23]-[26], neutralization lines [27]-[32], ground plane modifications [33]-[38], frequency-selective surface (FSS) or metasurface walls [39]-[42], metasurface corrugations or electromagnetic bandgap (EBG) structures [43], [44], and characteristic modes [45]-[48].

For an N-port antenna system, the complexity of the required $2N$-port tunable matching network becomes prohibitive as N increases. It is found that the perfect conjugate multiport impedance matching network is limited to narrow bandwidth [23] and is usually not achievable in practice [16]. A coupled resonator network was proposed in [24] to achieve broadband decoupling and matching for two non-directive antennas. Nevertheless, the coupled resonator network is mainly confined to two-port antennas.

Neutralization lines can be regarded as special decoupling networks, which cancel the coupling by introducing a second path with equal amplitude and opposite phase. As a result, most of the proposed neutralization lines in the literature are narrowband. A broadband neutralization line consisting of a circular disc and two strips was proposed in [32]. The circular disc enables multiple decoupling current paths with different lengths to cancel coupling currents on the ground plane at different frequencies. Nevertheless, the neutralization line is more suitable for the MIMO system with a small number of antenna elements, and is difficult to be excited for 700 MHz LTE handset MIMO arrays.

Various ground plane modifications provide band-stop filtering characteristics. Yet they are dedicated to specific antennas. A common approach is to make a slot in the ground plane in between the antennas. The slot can reduce the mutual coupling, yet may also increase the back radiation, e.g., [34].

Metasurface walls can effectively reduce the mutual coupling. Yet it is incompatible with low-profile antennas. Moreover, the metasurface wall can also affect the radiation pattern [39].

Most of the above works on handset MIMO antennas (except for [27], [28]) focus on the upper band. Decoupling for handset MIMO antennas in low-frequency bands is very challenging [84]. At low frequencies, the chassis does not only function as a ground plane, but also as a radiator shared by the multiple antenna elements. As result, isolation of MIMO antennas in compact terminals is typically less than 6 dB for frequencies below 1 GHz [51]. To avoid simultaneous excitation of the shared chassis by a two-port MIMO antenna, the position of the second antenna element can be moved to the middle of the chassis to efficiently reduce the chassis mode excitation [45]. Specifically, high isolation can be achieved by locating one electrical antenna (i.e., an antenna whose near-field are dominated by the electric field) along the short edge and the magnetic antenna (i.e., an antenna whose near-field are dominated by the magnetic field) at the opposite short edges [46]. In practice, it may not be possible to freely locate an antenna element, e.g., to the middle of the mobile chassis. And the antenna element that does not excite the chassis is usually band limited. To solve this problem, the metallic bezel of the mobile phone can be utilized for another feasible characteristic mode [47]. Nevertheless, the characteristic mode theory is more suitable for analyzing handset MIMO antennas.

Almost all of the above-mentioned works deal with handset MIMO antennas with a few antenna ports. Only a few studies have been carried out to tackle the mutual coupling problems for massive MIMO antennas for base stations. In the next subsection, we present some of the recent decoupling techniques for massive MIMO antennas.

B. DECOUPLING FOR MASSIVE MIMO ANTENNAS

Massive MIMO is the extension of the conventional MIMO technology, which exploits the directivity of a MIMO array with a large element number as one more dimension of freedom. Massive MIMO is also one of the key technologies for the 5G communication system, which is mainly utilized for base stations. In this subsection, we focus on the review of recent mutual coupling reduction methods in massive MIMO base station antennas, which has seldom been summarized before. Please note that the decoupling techniques in massive MIMO antennas have not been developed for many years. It is very challenging and literature on this topic is still very limited until now. In a massive MIMO base station antenna system, the mutual

coupling between antenna elements has to be lower than -30 dB according to the thumb of rules in the industry.

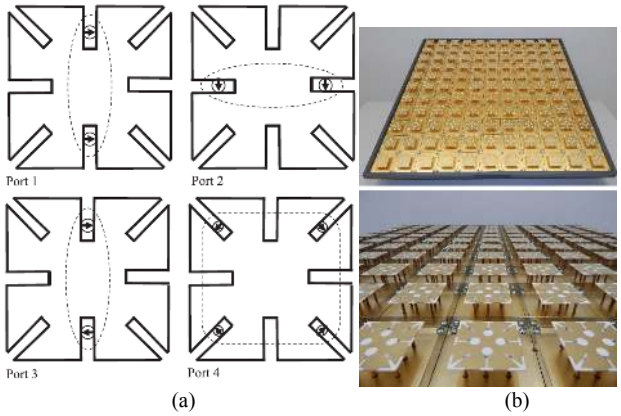

FIGURE 14. **Broadband massive MIMO in [88]: (a) different gap-source combinations for four antenna ports, and (b) prototype with 121 elements and 484 ports.**

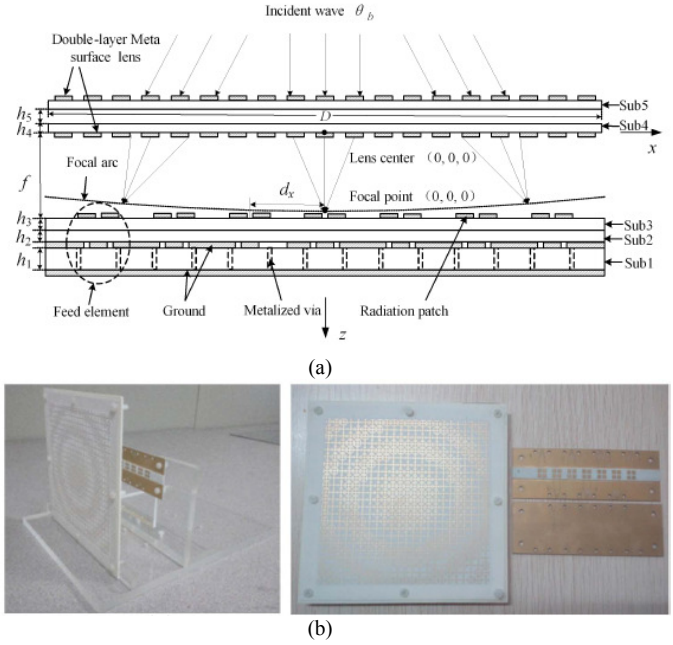

FIGURE 15. **Metamaterial-based thin planar lens massive MIMO in [89]: (a) the lens with seven-element feed array, and (b) prototype of the lens and seven-element feed array.**

An early investigation of massive MIMO antenna designs was carried out from 2015 in [85]. The authors in [85] develop a canonical two-port antenna that can be repeated and concatenated together to construct MIMO antenna arrays with arbitrary even numbers. The two-port antenna consists of two compact folded slots as the MIMO elements, and a parasitic element for decoupling. Furthermore, the coupling between the neighboring canonical elements (or two-port antennas) can also be reduced by properly designing the decoupling parasitic elements. A 20-port MIMO antenna has been proposed as one example. However, the massive MIMO array has the isolation between elements better than 10 dB instead of 30 dB. The total efficiency of each element is only around 30% within the operating bands and the elements have single polarization. All of these drawbacks limit the application of this design in practice. A dual polarized stacked patch antenna has been introduced in [86] with high gain and low mutual coupling between the two polarization ports. Several stacked patches are printed on a ring-shaped ground plane so that each patch points in a different direction. Three rings of stacked patches are placed upon each other to form a 3D structure. There are 144 ports in total in this massive MIMO array. As all the patches are pointing in different directions., the stacked patches have low mutual coupling and the isolation between elements are higher than 35 dB within the target bands. Dual slant polarized cavity-backed antennas have been applied to form a massive MIMO array in [87] with a 2D structure. However, the mutual coupling in this designed is suppressed well and the isolation is only better than 13 dB.

In [88], four different characteristic modes can be excited on each antenna element by four ports. Since different characteristic modes are orthogonal to each other, four ports have low mutual coupling. In 14 (a), each mode requires a gap-source combination in order to efficiently excite, and different gap-source combinations for four antenna ports are illustrated. 121 elements are placed on one big ground plane, as shown in Fig. 14 (b). The element distance is about 0.58 wavelength, so the isolation between elements is high. Since each element has four ports, there are 484 ports in total in the final prototype. The mutual coupling between the ports is better than -25 dB within a wideband.

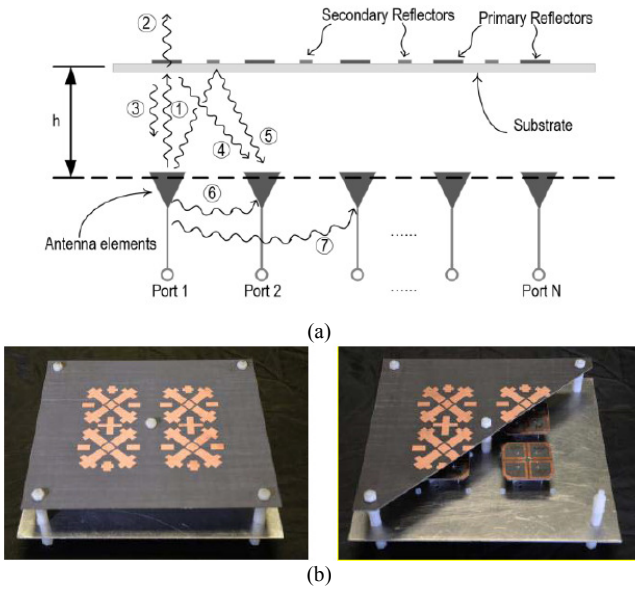

FIGURE 16. **Massive MIMO with decoupling surface in [90]: (a) sketch of the decoupling surface, and (b) prototype of a MIMO array with decoupling surface.**

Using metamaterial-based thin planar lens is considered as a low-cost and efficient way to realize massive MIMO

arrays [89]. As illustrated in Fig. 15 (a), different element feeds can be placed close to the focal arc of the metamaterial-based thin planar lens. The quasi-spherical wave (low gain) from different-element feeds will be transformed into quasi-plane wave (high gain) pointing in different directions. Only by switching between the element feeds, the beam can steer with high gain. The prototype of this antenna is given in Fig. 15 (b). The mutual coupling between the seven element feeds is lower than -30 dB. However, in Fig. 15 (b), it can also find that a distance between the meta-lens and element feeds are required, and this distance is large. Some more researches should be carried out to reduce lens-feed distance in order to realize the very compact configuration.

Very recently, a so-called array-antenna decoupling surface (ADS) has been proposed for massive MIMO antennas [90]. The ADS is a thin substrate layer consisting of small metal patches and placed above the MIMO antenna. By carefully designing the metal patches, the partially diffracted waves from the ADS can be controlled to cancel the unwanted coupled waves and the antenna pattern distortion can be kept at an acceptable level, as demonstrated in Fig. 16 (a). Fig. 16 (b) shows the prototype. This method is very promising and feasible to be applied to different types of antennas. The measured mutual coupling is lower than -30 dB with a small inter-element distance. However, the decoupling method in [90] is only applied for a 2 by 2 array. It can be expected that the patch patterns on ADS will be very complicated if the array number increases.

V. CONCLUSION

In this review paper, we shows the mutual coupling effects on the characteristics of MIMO antennas. It is shown that the mutual coupling changes the self- and mutual-impedances of the array antenna and, therefore, affects the antenna mismatches and embedded radiation efficiencies. The radiation patterns are altered in the presence of mutual coupling. For a two-port antenna, the mutual coupling tends to make the antenna patterns orthogonal to each other (i.e., the two antenna elements tend to radiate in opposite directions). As a result, correlations are also affected by the mutual coupling. Therefore two common interpretations of this effect. Comparing correlations with and without mutual coupling effects, it is shown that the correlation with mutual coupling effect is lower than that when the mutual coupling effect is ignored. Hence, one can claim that the mutual coupling tends to reduce the correlation. On the other hand, it is shown that, when the mutual coupling effect is taken into account, the correlation tends to reduce as the antenna separation decreases. As the mutual coupling effect becomes stronger at small antenna separation, others may also claim the mutual coupling increases the correlation. These two seemly contradicting claims are just two aspects of the same physical phenomenon. It is shown that mutual coupling below -10 dB has negligible effect on the capacity or error rate performance of the MIMO system. Nevertheless, when considering the PA nonlinearity, the OOB emission can be reduced by reducing the mutual coupling (even for mutual coupling below -28 dB). The mutual coupling effects can be partially mitigated in post processing by calibrating the mutual coupling from the received voltage. However, the SINR cannot be improved by post processing. In order to achieve the optimal performance, the mutual coupling has to be mitigated in the design of the array antenna. Many mutual coupling reduction techniques have been proposed in the literature. However, most of them are limited to two-port antennas. This paper presents several promising mutual coupling reduction techniques for massive MIMO antennas at base stations in the end.

REFERENCES

[1] C. J. Foschini, "Layered space-time architecture for wireless communication in a fading environment when using multi-element antennas," *Bell Labs Tech. Journal*, vol. 1, pp. 41-59, 1996.
[2] F. Rusek, D. Persson, B. K. Lau, *et al*., "Scaling up MIMO: opportunities and challenges with very large arrays," *IEEE Signal Process. Mag.*, vol. 30, no. 1, pp. 40–60, Jan. 2013.
[3] J. Zhang, X. Xue, E Björnson, *et al.* "Spectral efficiency of multipair massive mimo two-way relaying with hardware impairments," *IEEE Wireless Commun. Lett.*, 2017.
[4] B. Ai, K. Guan, R. He, *et al.*, "On Indoor Millimeter Wave Massive MIMO Channels: Measurement and Simulation," ***IEEE** J. Sel. Areas Commun.*, vol. 35, no. 7, pp.1678-1690, July 2017.
[5] Q. Yuan, Q. Chen, and K. Sawaya, "Performance of adaptive array antenna with arbitrary geometry in the presence of mutual coupling," *IEEE Trans. Antennas Propag.*, vol. 54, no. 7, pp. 1991-1996, Jul. 2006.
[6] B. Wang, Y. Chang and Y. Sun, "Performance of the large-scale adaptive array antennas in the presence of mutual coupling," *IEEE Trans. Antennas Propag.,* vol. 64, no. 6, pp. 2236-2245, June, 2016.
[7] Y. Wu, J. W. M. Bergmans, and S. Attallah, "Effects of antenna correlation and mutual coupling on the carrier frequency offset estimation in MIMO systems," *Int. Conf. Wireless Commun. Netw. Mobile Computing (WiCOM)*, Chengdu, China, 23-25 Sept. 2010.
[8] S. Lu, H. T. Hui, M. E. Bialkowski, *et al*., "The effect of antenna mutual coupling on channel estimation of MIMO-OFDM systems," *IEEE Antennas Propag. Society Int. Symp*., Honolulu, HI, Jun. 2007, pp. 1-4.
[9] H. S. Lui and H. T. Hui, "Mutual coupling compensation for direction-of-arrival estimations using the receiving-mutual impedance method," *Int. J. Antennas Propag*., vol. 2010, pp. 1-7, 2010.
[10] D. M. Pozar, "A relation between the active input impedance and the active element pattern of a phased array," *IEEE Trans. Antennas Propag.,* vol. 51, no. 9, pp. 2486-2489, Sep. 2003.
[11] L. Savy and M. Lesturgie, "Coupling effects in MIMO phased array," *IEEE* Radar Conference, Philadelphia, USA, May 2016, pp. 1-6.
[12] C. Fager, X. Bland, K. Hausmair, *et al.* "Prediction of smart antenna transmitter characteristics using a new behavioral modeling approach," *IEEE MTT-S Int. Microw. Symp.*, Tampa, FL, Jun. 1-6, 2014, pp. 1-4.
[13] X. Chen, S. Zhang, and A. Zhang, "On MIMO-UFMC in the presence of phase noise and antenna mutual coupling," *Radio Sci.*, vol. 52, 2017.
[14] K.-H. Chen and J.-F. Kiang, "Effect of mutual coupling on the channel capacity of MIMO systems," *IEEE Trans. Veh. Technol.,* vol. 65, no. 1, pp. 398-403, Jan. 2016.

[15] C. Masouros, M. Sellathurai and T. Ratnarajah, "Large-scale MIMO transmiters in fixed physical spaces: the effect of transmit correlation and mutual coupling," *IEEE Trans. Commun.,* vol. 61, no. 7, pp. 2794–2804, July 2013.
[16] L. Sun, P. Li, M. R. McKay, and R. D. Murch, "Capacity of MIMO systems with mutual coupling: transmitter optimization with dual power constraints," *IEEE Trans. Signal Process.*, vol. 60, no. 2, pp. 848-861, Feb. 2012.
[17] H. T. Hui, K. Y. Chan, and K. N. Yung, "Compensating for the mutual coupling effect in a normal-mode helical antenna array for adaptive nulling," *IEEE Trans. Veh. Technol.*, vol. 52, pp. 743–751, Jul. 2003.
[18] K. R. Dandekar, H. Ling, and G. Xu, "Experimental study of mutual coupling compensation in smart antenna applications," *IEEE Trans. Wireless Commun.*, vol. 1, no. 3, pp. 480–487, Jul. 2002.
[19] K. Karlsson and J. Carlsson, "Circuit based optimization of radiation characteristics of single and multi-port antennas", *Radioengineering*, vol. 18, no. 4, pp. 1513-1516 , 2009.
[20] A. Recioui and H. Bentarzi, "Genetic algorithm based MIMO capacity enhancement in spatially correlated channels including mutual coupling," *Wireless Personal communications*, vol. 63, no. 3, pp. 689-701, 2012.
[21] A. Recioui and H. Bentarzi, "Capacity optimization of MIMO wireless communication systems using a hybrid genetic-taguchi algorithm," *Wireless Personal Communications*, vol. 71, no. 2, pp. 1003-1019, 2013.
[22] A. Recioui, "Application of a galaxy-based search algorithm to MIMO system capacity optimization," *Arabian Journal for Science and Engineering*, vol. 41, no. 9, pp. 3407-3414, 2016.
[23] B. K. Lau, J. B. Andersen, G. Kristensson, and A. F. Molish, "Impact of matching network on bandwidth of compact antenna arrays," *IEEE Trans. Antennas Propag.*, vol. 54, no. 11, pp. 3225–3238, Nov. 2006.
[24] L. Zhao, L. K. Yeung, and K.-L. Wu, "A coupled resonator decoupling network for two-element compact antenna arrays in mobile terminals," *IEEE Trans. Antennas Propag.*, vol. 62, no. 5, pp. 2767–2776, May 2014.
[25] B. Pan and T. Cui, "Broadband decoupling network for dual-band microstrip patch antennas," *IEEE Trans. Antennas Propag.*, in press.
[26] C.-H. Wu, C.-L. Chiu, and T.-G. Ma, "Very compact fully lumped decoupling network for a coupled two-element array," *IEEE Antennas Wireless Propag. Lett.*, vol. 15, pp. 158-161, 2016.
[27] Y. Ban, Z. Chen, Z. Chen, K. Kang, and J. L.-W. Li, "Decoupled hepta-band antenna array for WWAN/LTE smartphone applications," *IEEE Antennas Wireless Propag. Lett.*, vol. 13, pp. 999-1002, 2014.
[28] L. Li, F. Huo, Z. Jia, and W. Han, "Dual zeroth-order resonance antennas with low mutual coupling for MIMO communications," *IEEE Antennas Wireless Propag. Lett.*, vol. 12, pp. 1692-1695, 2013.
[29] S.-W. Su, C.-T. Lee, and F.-S. Chang, "Printed MIMO-antenna system using neutralization-line technique for wireless USB-dongle applications," *IEEE Trans. Antennas Propag.*, vol. 60, no. 2, pp. 456–463, Feb. 2012.
[30] A. Diallo, C. Luxey, P. L. Thuc, *et al.*, "Study and reduction of the mutual coupling between two mobile phone pifas operating in the DCS1800 and UMTS bands," *IEEE Trans. Antennas Propag.*, vol. 54, no. 11, pp. 3063–3074, Nov. 2006.
[31] H. Wang, L. Liu, Z. Zhang, *et al.*, "Ultra-compact three-port MIMO antenna with high isolation and directional radiation patterns," *IEEE Antennas Wireless Propag. Lett.*, vol. 13, pp. 1545-1548, 2014.
[32] S. Zhang and G. F. Pedersen, "Mutual coupling reduction for UWB MIMO antennas with a wideband neutralization line," *IEEE Antennas Wireless Propag. Lett.*, vol. 15, pp. 166-169, 2016.
[33] C.-Y. Chiu, C.-H. Cheng, R. D. Murch, and C. R. Rowell, "Reduction of mutual coupling between closely-packed antenna elements," *IEEE Trans. Antennas Propag.*, vol. 55, no. 6, pp. 1732–1738, Jun. 2007.
[34] J. Yang, F. Yang, and Z. Wang, "Reducing mutual coupling of closely spaced microstrip mimo antennas for WLAN application," *IEEE Antennas Wireless Propag. Lett.*, vol. 10, pp. 310-313, 2011.
[35] J. Li, Q. Chu, Z. Li, and X. Xia, "Compact dual band-notched UWB MIMO antenna with high isolation," *IEEE Trans. Antennas Propag.*, vol. 61, no. 9, pp. 4759–4766, Sep. 2013.
[36] L. Liu, S. W. Cheung, and T. I. Yuk, "Compact MIMO antenna for portable devices in UWB applications," *IEEE Trans. Antennas Propag.*, vol. 61, no. 8, pp. 4257–4264, Aug. 2013.
[37] S. Zhang, B. K. Lau, Y. Tan, *et al.*, "Mutual coupling reduction of two PIFAs with a T-shape slot impedance transformer for MIMO mobile terminals," *IEEE Trans. Antennas Propag.*, vol. 60, no. 3, pp. 1521–1531, Mar. 2012.
[38] C. T. Lee and K. L. Wong, "Internal WWAN clamshell mobile phone antenna using a current trap for reduced ground plane effects," *IEEE Trans. Antennas Propag.*, vol. 57, no. 10, pp. 3303–3308, Oct. 2009.
[39] A. Dadgarpour, B. Zarghooni, B. S. Virdee, T. A. Denidni, and A. A. Kishk, "Mutual coupling reduction in dielectric resonator antennas using metasurface shield for 60-GHz MIMO systems," *IEEE Antennas Wireless Propag. Lett.*, vol. 16, pp. 477-480, 2017.
[40] G. Zhai, Z. N. Chen, and X. Qing, "Enhanced isolation of a closely spaced four-element MIMO antenna system using metamaterial mushroom," *IEEE Trans. Antennas Propag.*, vol. 63, no. 8, pp. 3362–3370, Aug. 2015.
[41] M. Akbari, H. A. Ghalyon, M. Farahani, *et al.*, "Spatially decoupling of CP antennas based on FSS for 30-GHz MIMO systems," *IEEE Access*, vol. 5, pp. 6527-6537, 2017.
[42] R. Karimian, A. Kesavan, M. Nedil, and T. A. Denidni, "Low-mutual-coupling 60-GHz MIMO antenna system with frequency selective surface wall," *IEEE Antennas Wireless Propag. Lett.*, vol. 16, pp. 373-376, 2017.
[43] S. Gupta, Z. Briqech, A. R. Sebak, and T. A. Denidni, "Mutual-coupling reduction using metasurface corrugations for 28 GHz MIMO applications," *IEEE Antennas Wireless Propag. Lett.*, in press.
[44] F. Yang and Y. Rahmat-Samii, "Microstrip antennas integrated with electromagnetic band-gap (EBG) structures: A low mutual coupling design for array applications," *IEEE Trans. Antennas Propag.,* vol. 51, no.10, pp. 2936–2946, Oct. 2003.
[45] H. Li, Y. Tan, B. K. Lau, Z. Ying, and S. He, "Characteristic mode based tradeoff analysis of antenna-chassis interactions for multiple antenna terminals," *IEEE Trans. Antennas Propag.*, vol. 60, no. 2, pp. 409–502, Feb. 2012.
[46] H. Li, B. K. Lau, Z. Ying, and S. He, "Decoupling of multiple antennas in terminals with chassis excitation using polarization diversity, angle diversity and current control," *IEEE Trans. Antennas Propag.*, vol. 60, no. 12, pp. 5947–5957, Dec. 2012.
[47] H. Li, Z. T. Miers, and B. K. Lau, "Design of orthogonal MIMO handset antennas based on characteristic mode manipulation at frequency bands below 1 GHz," *IEEE Trans. Antennas Propag.*, vol. 62, no. 5, pp. 2756–2766, May 2014.
[48] M. Bouezzeddine and W. L. Schroeder, "Design of a wideband, tunable four-port MIMO antenna system with high isolation based on the theory of characteristic modes," *IEEE Trans. Antennas Propag.*, vol. 64, no. 7, pp. 2679–2688, Jul. 2016.
[49] M. T. Ivrlac and J. A. Nossek, "Toward a circuit theory of communication," *IEEE Trans. Circuits Syst*., vol. 57, no. 7, Jul. 2010.
[50] Y. Fei, Y. Fan, B. K. Lau, and J. S. Thompson, "Optimal single-port matching impedance for capacity maximization in compact MIMO arrays", *IEEE Trans. Antennas Propag*., vol. 56, no. 11, pp. 3566-3575, Nov. 2008.
[51] V. Plicanic, B. K. Lau, A. Derneryd, and Z. Ying, "Actual diversity performance of a multiband diversity antenna with hand and head effects," *IEEE Trans. Antennas Propag*., vol. 57, no. 5, pp. 1547-1556, May, 2009.

[52] H. M. Aumann, A. J. Fenn, and F. G. Willwerth, "Phased array antenna calibration and pattern prediction using mutual coupling measurements," *IEEE Trans. Antennas Propag*., vol. 37, no. 7, pp. 844–850, Jul. 1989.
[53] H. Wei, D. Wang, H. Zhu, et al., "Mutual coupling calibration for multiuser massive MIMO systems," *IEEE Trans.Wireless Commun.*, vol. 15, no. 1, pp. 606–619, Jan. 2016.
[54] C. Craeye and D. González-Ovejero, "A review on array mutual coupling analysis," *Radio Sci*., vol. 46, no. 2, pp. 1-25, Apr. 2011.
[55] H. Singh, H. Sneha, and R. Jha, "Mutual coupling in phased arrays: A review," *Int. J. Antennas Propag*., vol. 2013, pp. 1–23, 2013.
[56] J. L. Allen and B. L. Diamond, "Mutual Coupling in Array Antennas," *Technical Report* EDS-66–443, Lincoln Lab., MIT, October 4, 1966.
[57] C. A. Balanis, *Antenna Theory: Analysis and Design*, 3rd edition John Wiley & Sons, 2005.
[58] W. Wasylkiwskyj and W. K. Kahn, "theory of mutual coupling among minimum-scattering antennas", *IEEE Trans. Antennas Propag*., vol. 18, no. 2, pp. 204-216, Mar., 1970.
[59] P.-S. Kildal and K. Rosengren, "Electromagnetic analysis of effective and apparent diversity gain of two parallel dipoles," *IEEE Antennas Wireless Propag. Lett.,* vol. 2, pp. 9-13, 2003.
[60] X. Chen, "Experimental investigation of the number of independent samples and the measurement uncertainty in a reverberation chamber," *IEEE Trans. Electromagn. Compat.,* vol. 55, no. 5, pp. 816-824, Oct. 2013.
[61] E. Jorswieck and H. Boche, "Majorization and Matrix-Monotone Functions in Wireless Communications," *Foundations Trends Commun. Inf. Theory*, vol. 3, no. 6, pp. 553–701, 2006.
[62] B. T. Quist and M. A. Jensen, "Optimal antenna radiation characteristics for diversity and MIMO systems," *IEEE Trans. Antennas Propag.*, vol. 57, no. 11, pp. 3474-3481, Nov. 2009.
[63] R. G. Vaughan and J. B. Andersen, "Antenna diversity in mobile communications", *IEEE Trans. Vehic. Technol.* vol. 36, no. 4, pp. 149-172, Nov. 1987.
[64] J. W. Wallace and M. A. Jensen, "Termination-dependent diversity performance of coupled antennas: network theory analysis", *IEEE Trans. Antennas Propag.,* vol. 52, no. 1, pp. 98-105, Jan. 2004.
[65] T. Svantesson and A. Ranheim, "Mutual coupling effects on the capacity of multielement antenna systems," *ICASSP*, Salt Lake, UT, May 2001, pp. 2485 – 2488.
[66] R. Janaswamy, "Effect of element mutual coupling on the capacity of fixed length linear arrays," *IEEE Antennas Wireless Propag. Lett.,* vol. 1, pp. 157-160, 2002.
[67] W. Fan, P. Kyösti, Y. Ji, *et al.*, "Experimental evaluation of user influence on test zone size in multi-probe anechoic chamber setups," *IEEE Access*, vol. 5, pp. 18545-18556, 2017.
[68] X. Chen, "Throughput modeling and measurement in an isotropic-scattering reverberation chamber," *IEEE Trans. Antennas Propag*., vol. 62, no. 4, pp. 2130-2139, April 2014.
[69] S.-J. Chern, W.-J. Huang, and H.-I Liu, "The effects of mutual coupling for the space-time block coded MIMO-OFDM systems," *Int. Symp. Intelligent Signal Process. Commun. Sys. (ISPACS)*, Phuket, Thailand, Oct. 2016, pp. 1-6.
[70] S. Lu, H. T. Hui, M. E. Bialkowski, *et al*., "BER performance of MIMO-OFDM systems with the existence of antenna mutual coupling," *IEEE Antennas Propag. Society Int. Symp*., Honolulu, HI, Jun. 2007, pp. 1-4.
[71] W. C. Y. Lee, "Mutual coupling effect on maximum-ratio diversity combiners and application to mobile ratio," *IEEE Trans. Commun. Technol*., vol. COM-18, pp. 779-791, Dec. 1970.
[72] Q. Wu, S. Guo, X. Chen, "A low-profile MIMO antenna with arc-loaded dipole elements for 698—2700 MHz LTE femtocell base stations," *IEEE Antennas Propag. Mag.*, in press.
[73] R. Tian, B. K. Lau, and Z. Ying, "Multiplexing efficiency of MIMO antennas," *IEEE Antennas Wireless Propag. Lett.*, vol. 10, pp. 183-186, 2011.
[74] X. Chen, P.-S. Kildal, J. Carlsson, and J. Yang, "MRC diversity and MIMO capacity evaluations of multi-port antennas using reverberation chamber and anechoic chamber," *IEEE Trans. Antennas Propag*., vol. 61, no. 2, pp. 917-926, Feb. 2013.
[75] J. Meinilä, P. Kyösti, L. Hentilä, et al., D5.3: *WINNER+ Final Channel Models*, WINNER+.
[76] D. He, K. Guan, A. Fricke, *et al.*, "Stochastic channel modeling for kiosk applications in the Terahertz band," *IEEE Trans. Terahertz Sci. Technol.*, vol. 7, no. 5, pp. 502-513, Sep. 2017.
[77] R. He, B. Ai, G. Stuber, *et al.*, "Geometrical based modeling for millimeter wave MIMO mobile-to-mobile channels," *IEEE Trans. Veh. Technol.*, in press, 2018.
[78] X. Chen and S. Zhang, "Multiplexing efficiency for MIMO antenna-channel impairment characterisation in realistic multipath environments," *IET Microw. Antennas Propag.*, vol. 11, no. 4, pp. 524-528, Apr. 2017.
[79] P. Kyösti, J. Meinilä, L. Hentilä, et al., *IST-4-027756 WINNER II D1.1.2 V1.2 WINNER II Channel Models: Part I Channel Models*, 2007.
[80] X. Chen, P.-S. Kildal, and J. Carlsson, "Revisiting the Complex Correlation in a MIMO System," in *Proc. 8th European Conference on Antennas and Propagation (EuCAP 2014)*, Hague, Netherlands, 6-11 April 2014, pp. 2735 - 2739.
[81] G. Z. El Nashef, F. Torres, S. Mons, T. Reveyrand, T. Monediere, E. Ngoya, and R. Quere, "EM/Circuit Mixed Simulation Technique for an Active Antenna," *IEEE Antennas Wireless Propag. Lett.*, vol. 10, pp. 354-357, 2011.
[82] P. Banelli and S. Cacopardi, "Theoretical analysis and performance of OFDM signals in nonlinear AWGN channels," *IEEE Trans. Commun.*, vol. 48, no. 3, pp. 430-441, Mar. 2000.
[83] M. Manteghi, and Y. Rahmat-Samii, "Multiport characteristics of a wide-band cavity backed annular patch antenna for multipolarization operations," *IEEE Trans. Antennas Propag.*, vol. 53, pp. 466 – 474, Jan. 2005.
[84] Z. Ying, C. Y. Chui, K. Zhao, S. Zhang, and S. He, "Antenna Design for Diversity and MIMO Application," *Handbook of Antenna Technologies*, pp. 1-43, Springer Singapore, 2014.
[85] S. Soltani and R. D. Murch, "A compact planar printed MIMO antenna design," *IEEE Trans. Antennas Propag*., vol. 63, no. 3, pp. 1140–1149, Mar. 2015.
[86] Y. Gao, R. Ma, Y. Wang, Q. Zhang, and C. Parini, "Stacked patch antenna with dual-polarization and low mutual coupling for massive MIMO," *IEEE Trans. Antennas Propag.*, vol. 64, no. 10, pp. 4544–4549, Oct. 2016.
[87] M. V. Komandla, G. Mishra, S. K Sharma, "Investigations on Dual Slant Polarized Cavity Backed Massive MIMO Antenna Panel with Beamforming," *IEEE Trans. Antennas Propag*., vol. 65, no. 12, pp. 6794–6799, Dec. 2017.
[88] D. Manteuffel and R. Martens, "Compact multimode multielement antenna for indoor UWB massive MIMO," *IEEE Trans. Antennas Propag.*, vol. 64, no. 7, pp. 2689–2697, Jul. 2016.
[89] M. Jiang, Z. N. Chen, Y. Zhang, W. Hong, X. Xuan, "Metamaterial-based thin planar lens antenna for spatial beamforming and multibeam massive MIMO," *IEEE Trans. Antennas Propag.*, vol. 65, no. 2, pp. 464-472, Feb. 2017.
[90] K.-L. Wu, C. Wei, X. Mei, and Z. Zhang, "Array-antenna decoupling surface" *IEEE Trans. Antennas Propag.*, vol. 65, no. 12, pp. 6728-6738, Dec. 2017.

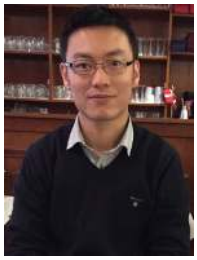

Xiaoming Chen (M'16) received the B.Sc. degree in electrical engineering from Northwestern Polytechnical University, Xi'an, China, in 2006, and M.Sc. and PhD degrees in electrical engineering from Chalmers University of Technology, Gothenburg, Sweden, in 2007 and 2012, respectively.

From 2013 to 2014, he was a postdoctoral researcher at the same University. From 2014 to 2017, he was with Qamcom Research & Technology AB, Gothenburg, Sweden. Since

2017, he has been a professor at Xi'an Jiaotong University, Xi'an, China. His research areas include MIMO antennas, over-the-air testing, reverberation chambers, and hardware impairments and mitigation.

He is a recipient of the 1000-Talent Plan for Young Scholars in China and serves as an Associate Editor for IEEE Antennas and Wireless Propagation Letters. He received the URSI (International Union of Radio Science) Young Scientist Award 2017.

Shuai Zhang received the B.E. degree from the University of Electronic Science and Technology of China, Chengdu, China, in 2007 and the Ph.D. degree in electromagnetic engineering from the Royal Institute of Technology (KTH), Stockholm, Sweden, in 2013.

After his Ph.D. studies, he was a Research Fellow at KTH. In April 2014, he joined Aalborg University, Denmark, where he currently works as Associate Professor. In 2010 and 2011, he was a Visiting Researcher at Lund University, Sweden and at Sony Mobile Communications AB, Sweden, respectively. He was also an external antenna specialist at Bang & Olufsen, Denmark from 2016-2017. His research interests include: mobile terminal mmwave antennas, biological effects, CubeSat antennas, UWB wind turbine blade deflection sensing, MIMO antenna systems, and RFID antennas.

Qinlong Li received the B.S. degree from Xi'an Jiaotong University, Xi'an, China, in 2010, and the M.S. degree from University of Chinese Academy of Sciences, Beijing, China, in 2013. He is currently working toward the Ph.D. degree at the department of electrical and electronic engineering, The University of Hong Kong, Hong Kong, China.

His research interests include antenna and metamaterial design.